PLASMA DIAGNOSTICS

INFLUENCE OF MAGNETIC FIELD ON SPECTRA OF ELECTROSTATIC OSCILLATIONS IN PLASMA E×*B*-DISCHARGE

© 2025 N. A. Strokin*, A. V. Rigin**

Irkutsk National Research Technical University, Irkutsk, Russia

**e-mail: strokin85@inbox.ru*

***e-mail: arseniy.rigin@mail.ru*

Received November 01, 2024

Revised December 19, 2024

Accepted December 22. 2024

Abstract. Simultaneous measurements of amplitude-frequency characteristics of oscillations at frequencies of 20 kHz–30 MHz of the discharge current derivative and ion current in the plasma of a self-sustained **E × ×B discharge** in an accelerator with an anode layer — under conditions of a strong inhomogeneous magnetic field (on the cathode, the radial component up to B_{rK} = 4200 G; on the anode up to B_{rA} = 1010 G) revealed both similar and different properties of oscillations of the discharge current derivative and ion current. Common features include a discrete spectrum and, mainly, the cluster nature of oscillations. Threshold values of the magnetic field B_{rA} = 660–720 G were discovered, at which a rapid increase in the frequency of oscillations with maximum amplitude occurs, up to $f_{\max} \sim 4.5$ MHz. At the same time, in the frequency range not exceeding 1 MHz, there are jumps of distinct peaks in the amplitude-frequency characteristic from tens of kHz to hundreds of kHz. Differences in the amplitude-frequency characteristics of discharge current and ion current oscillations include ~ 5 times lower frequencies of oscillations with maximum amplitude of the discharge current relative to the ion current at $205 \le B_{rA} \le 660$ G, a sharp decrease in $f_{\max}$ for the amplitude-frequency characteristic of the discharge current, but a sharp increase in $f_{\max}$ for the amplitude-frequency characteristic of ion current when B_{rA} becomes greater than 820 G. The results of measuring the characteristics are analyzed together with the plasma emission spectra measured in the same discharge modes in the wavelength range of 200–1100 nm and the ion energy distributions in the range of 50–1200 eV. Possible causes of discharge and ion current oscillations generation are discussed when modified two-stream and electron-cyclotron drift instabilities are excited in the **E × ×B discharge** plasma for frequencies $f \le 1$ MHz. The effect on ions is analyzed from the perspective of axial instability of the flow of unmagnetized ions at higher frequencies.

Keywords: *self-sustained discharge, crossed electric and magnetic fields, discharge current, ion current, electrostatic oscillations, amplitude-frequency characteristic*

DOI: 10.31857/S03672921250107e5

1. INTRODUCTION

For plasma discharges in crossed electric and magnetic fields with magnetized electrons and non-magnetized ions, based on the results of experimental work, theoretical studies, and numerical modeling, it was determined that electrostatic oscillations exist in the frequency range from several kHz to ~ 10^9 Hz and are limited by the highest of ω_{pe}, ω_{ce} frequencies (ω_{pe}, ω_{ce} — plasma and cyclotron electron frequencies). Fairly complete information about the history of oscillation research, types, and causes of their generation is contained in reviews [1–4]. In the introduction to our article, we will limit ourselves to considering experiments that have already been conducted. In the "Discussion of Results" section, we will refer to information from theoretical studies and modeling.

The papers [5-7] present the results of the first experiments on the study of electrostatic oscillations of ion current and floating potential in the plasma of a non-self-sustained **E ×B discharge** of a stationary plasma thruster — SPT. Two main types of oscillations that were observed are low-frequency (f_{LF} = 10–70 kHz) and high-frequency oscillations with $f_{HF} \leq 1$ MHz and a bandwidth $\Delta f \sim f_{HF} \sim v_0 / L$ (v_0 — ion velocity at the SPT output; L — channel length) were identified as azimuthal ionization oscillations (breathing oscillations) and longitudinal transit oscillations. We will not consider ionization oscillations in detail, since in our case, in the plasma of an accelerator with anodic layer (accelerator with anodic layer — AAL) and a self-sustained discharge in neon, the instability associated with "burnout of neutrals" does not develop, as the degree of ionization η in AAL is low: at operating pressure ~ 10^{-4} Torr, ion density $n_i \sim 10^7$ cm^{-3}, $\eta = n_i / n_0 \sim 10^{-4}$. In addition, we exclude from consideration oscillations with frequencies $f \leq 20$ kHz, eliminating the contribution of possible circuit oscillations determined by the AAL power supply circuit.

Increasing the magnetic field from 100 to 260 G led to a broadening of the amplitude-frequency characteristic (AFC) of the azimuthal electric field oscillations toward higher frequencies — up to 200 MHz and a nonlinear growth in oscillation amplitude along the entire length of the discharge channel; at low fields, certain distinct frequencies were observed in the AFC [7]. Azimuthal oscillations of the ion current with frequencies up to 25 MHz were also investigated by the authors of [8]. The signals from the probes had a non-stationary character; the time-averaged amplitude of the oscillations did not correlate with any of the SPT operating parameters. The AFC showed a set of oscillation clusters, with widths at half-height $\Delta f \sim$ 1–3 MHz — "multiple waves with the same phase velocity and several wave numbers," possessing, quite precisely, multiple frequencies. An increase in the magnetic field led to a monotonic decrease in oscillation frequency. The burst-like nature of

signals from floating probes and the AFC of azimuthal oscillations in the high-frequency range (5–150 MHz) was also demonstrated in works [9, 10].

Taking into account plasma inhomogeneity – $d(H_0 / n_0)/dx \neq 0$ $dH_0/dx \neq 0$ (H_0, n_0 — maximum radial magnetic field strength and plasma density; x — longitudinal coordinate) led the authors of [11] to conclude about the possibility of exciting drift instability with frequencies $\omega_{ci} \ll \omega \ll (\omega_{ce}, \omega_{pe})$. Probe measurements of the floating potential in the near-wall xenon plasma in SPT revealed the dependence of AFC on the magnetic field magnitude. At $H < H_{opt} \approx 170$ G (H_{opt} — the field at which the discharge current and ion current were maximum) — this is a sequence of multiple peaks with a first harmonic frequency f = 2–5 MHz and a maximum frequency $f_{\max} \sim 15$ MHz. The authors identified these oscillations as azimuthal electron drift waves. At $H > 170$ G, the AFC is a single frequency-wide peak in the same frequency range [11].

Regarding transit oscillations, we will also not consider them when interpreting the results, since ion energy spectra in AAL are broad: from ~ 50 eV to ~ 1.2 eU_d (U_d — discharge voltage), therefore the spectrum of oscillation frequencies, within the framework of transit instability, turns out to be continuous, which does not correspond to experimental results.

Plasma accelerators with anode layer have not found widespread use as spacecraft engines, but are universally used as ion sources in vacuum surface cleaning installations, ion sputtering for producing thin-film objects, precise surface finishing, modification of surface properties of materials — for carrying out ion-beam technology operations. In our case, AAL is an element of a plasma-optical mass separator prototype — a source of a multicomponent ion beam. Oscillations of discharge and ion currents will obviously affect the quality of mass separation of ions, so it is necessary to know the frequencies and patterns of amplitude-frequency response changes when varying discharge parameters. An external cathode — usually a plasma electron source can contribute to the amplitude-frequency response **E ×B** of a non-self-sustained discharge, therefore it was not used in our work and a self-sustained **E ×B** discharge was implemented in the AAL. discharge.

In the proposed work, we measured the spectra of electrostatic plasma oscillations of a self-sustained anomalous (growing current-voltage characteristic) glow **E ×B** discharge in a plasma accelerator with anode layer at frequencies of 20 kHz–30 MHz while changing the induction of a non-uniform magnetic field in a wide range of values: radial (main on the discharge chamber axis) component at the anode $B_{rA} \approx$ 200–1100 G; while at the AAL cathode $B_{rK} \approx$ 800–4200 G. The discharge voltage varied from 500 to 2000 V. Neon with an inlet rate of q_{Ne} = 100 cm^3/min was used as the plasma-forming gas. The results of measuring oscillation spectra — amplitude-frequency

responses were correlated with the ion energy distributions measured in the same discharge modes in the range of 50–1200 eV and plasma emission spectra in the wavelength range of 200–1100 nm.

2. SETUP

Plasma was generated in AAL. Fig. 1a shows a schematic of the **E ×B** discharge region in AAL. The magnetic field in the anode-cathode gap was created using two axially located coils inside the AAL; Fig. 1b shows an example of the radial component distribution of the magnetic field B_r along the axis of the discharge gap.

3. DIAGNOSTICS

The study of plasma oscillations was conducted non-invasively. The discharge current perturbation was monitored by the derivative of the discharge current, which was measured using a shielded induction sensor - a Rogowski coil without an integrating circuit, embracing the anode-cathode power supply circuit of the AAL near the anode [12]. It was assumed that in the case of harmonic oscillations, the frequencies of current oscillations and its derivative are the same. Only the variable component of ion current oscillations was recorded - the signal from the ion collector of the analyzer with retarding potential (RPA) [13] was fed to the oscilloscope input through an isolation transformer. Both signals were recorded simultaneously on different channels of a digital oscilloscope at a sweep of 100 μs/div (frequency resolution 1 kHz) or 2.5 μs/div (frequency resolution 40 kHz). The Rogowski coil does not distort the shape and frequency of the signal in the range of 25 kHz-30 MHz. The ion current was taken from the RPA collector when the potential on its separation grid was zero, and a potential of -20 V was maintained on the analyzing grid. The isolation transformer does not distort the shape and frequency of the signal from 3 kHz to 30 MHz. Processing of signals from both sensors was carried out in a program we created, which allows visualization of signals from two oscilloscope channels on one panel, plotting frequency response characteristics (from one to five) and comparing them with the ability to determine both frequency and amplitude for each point of the frequency response [14].

The RPA was installed at the cathode exit of the AAL on the axis of the discharge chamber - it recorded the ion energy distributions integrated along the length of the discharge gap. The analyzing voltage was increased stepwise with a step of 1-20 V with a hold at each step of 10 ms (time resolution). The operation of the RPA was controlled by a hardware-software complex [15].

Plasma emission spectra were recorded using a CCS200 spectrometer, the optical fiber cable of which was installed at the output of the AAL cathode. Thus, it registered the spectrum of radiation

integrated along the length of the discharge gap. The wavelength resolution of CCS200 $\Delta\lambda$ = 1.1 nm; the spectra were time-integrated over the optical signal accumulation period $\Delta t \sim 1$ s.

4. EXPERIMENTAL RESULTS

4.1. Oscillations of the discharge current derivative

The frequencies of discharge current oscillations with maximum amplitudes f_{max}, at magnetic fields of 205 G $\leq B_{rA} \leq$ 650 G were equal to 160-280 kHz (Fig. 2, curve *1*). When 720 G $\leq B_{rA} \leq$ 820 G the frequency $f_{max} \sim$ 4 MHz, and when $B_{rA} \geq$ 820 G, oscillations with maximum amplitude return to values of 150-200 kHz.

The amplitude-frequency spectrum of discharge current oscillations consists of a set of many frequencies. Fig. 3 (curve *1*) shows the frequency response of the signal from the Rogowski coil, which highlights oscillations with a frequency of 211 kHz (maximum amplitude), with an amplitude an order of magnitude lower at frequencies ~ 400, 485, 723 kHz, a cluster of oscillations with frequencies from 4.5 to 7 MHz, "traces" at frequencies ~ 20 MHz. The "two-beam" frequency response is preserved when changing B_{rA} in the range of 344-910 G with an increase in the amplitude of lower-frequency oscillations by about an order of magnitude. The frequency response shown in Fig. 3 (curve *1*) is constructed from signals that have irregular bursts of high-frequency oscillations, better distinguished on the ion signal (10-12 oscillation periods) and manifesting on the signal from the Rogowski coil (Fig. 4a, b). Oscillation bursts can also have a regular character (Fig. 4c, d).

Changing conditions for **E ×B** discharge can lead to the disappearance of bursts and the appearance of a regular signal, the frequency response of which consists of bursts at selected (mono) frequencies (Fig. 5).

With small changes in the magnetic field, "jump-like" changes in the frequency response of discharge current oscillations are possible, as illustrated in Fig. 6. Until $B_{rA} <$ 660 G, there were no noticeable oscillations of the discharge current. At $B_{rA} =$ 660 G a peak appeared at a frequency of $f_1 \approx$ 43 kHz. Increasing B_{rA} to 720 G led to the disappearance of oscillations at frequency f_1 and the appearance of oscillations at $f_2 \approx$ 331 kHz. The next threshold magnetic field was the value of B_{rA} 100 G higher, which led to the disappearance of narrow-frequency frequency responses and the appearance of a wide-frequency cluster of oscillations in the range of 150-220 kHz. The cluster nature of discharge current oscillations persists up to 968 G (no measurements beyond that) both for frequencies ~ of hundreds of kHz, and for frequencies ~ of 4-5 MHz. The fine structure of the frequency response is well distinguished for frequency response-2 in Fig. 6.

4.2. Ion current oscillations

The nature of the change in the frequency having the maximum amplitude for induction current and ion signals with changing magnetic field (Fig. 2) can be called the same up to $B_{rA} \approx 820$ G, and beyond that f_{max} of the ion current rapidly increases, while the frequency having the maximum amplitude for the discharge current decreases. The frequency response of the ion signal in the frequency range $f \geq 1$ MHz is "richer" compared to the frequency response of discharge current oscillations. Thus, in Fig. 3 (curve *2*), clusters are visible around frequencies of 119, 320 kHz; 4.2; 5; 6.4; 7.6 MHz, which, to a certain extent, correspond to the frequencies of discharge current oscillations, but clusters around 9; 10.4; 11; 16.8; 17; 18; 18.8; 19.3 MHz are oscillations to which only ions are sensitive.

The evolution of signal types from the ion collector (Fig. 4b, 4d, 5a) determines the diversity of frequency responses. Fig. 7 shows five frequency responses of ion current oscillations for $f \geq 4$ MHz with changes in B_{rA} from 470 to 870 G. Common features of the oscillations are a set of frequencies, clusters, bursts at selected frequencies both far from the clusters and within the cluster of oscillations.

In the frequency range $f \leq 1$ MHz, the determining role of the magnetic field in the generation of ion current oscillations is also visible. Interesting events occur when the magnetic field changes from 660 to 720 G: the distinct oscillation peaks at 43 and 87 kHz (660 G) "transform" into peaks at frequencies of 331 and 622 kHz (Fig. 8, frequency response curves *1* and *2*). And further - beyond the threshold of 720 G up to $B_{rA} \approx 910$ G, there are no explicit ion signals, with the discharge currents being maximum in the series (in Fig. 8, frequency response curves *3* and *4*).

5. JOINT DATA ANALYSIS

The magnetic field in the **E × B** zone of the AAL discharge determines changes not only in the spectra of electrostatic plasma oscillations but also in the ion energy distribution and plasma radiation spectra. Figure 9 shows the energy spectra of ions and ion density (inset) calculated from these spectra. Significant changes in distributions occur during the transition of B_{rA} from 470 G (curve *2* ; maximum ion density) to 660 G (curve *3*): the amplitude decreases and the most probable energy W increases by approximately 150 eV. This corresponds to a decrease in ion density (area under the curve dI / dW) by 2.8 times.

For frequencies $f \geq 4$ MHz, the transition of B_{rA} from 470 to 660 G leads to the generation of distinct peaks in ion current oscillations (Fig. 7, curves *2–4*). At the same time, the level of oscillations in clusters changes slightly. In the range of 30-700 kHz at fields of 660 and 720 G, single bursts are

also observed on the "ionic" frequency response curves (Fig. 8, curves *1* , *2*). Further growth of B_{rA} leads to the disappearance of bursts and a decrease in the oscillation level (Fig. 8, curves *3* , *4*). At all recorded frequencies, ion oscillations are most prominently manifested in the MHz range.

As previously noted, until $B_{rA} < 660$ G, no discharge current oscillations were registered. At $B_{rA} \geq 660$ G, they appeared at various distinct frequencies, subsequently transitioning to a "cluster" type frequency response at 720 G. The cluster nature of the frequency response (not a set of harmonics with multiple frequencies) apparently reflects the integral nature of the signal in both azimuthal and axial directions across the entire discharge gap, but with a distinct oscillation excitation zone.

Comparison of events during the transition from 470 G $\rightarrow$ 660 G for ion energy distributions and frequency response of ion oscillations leads to the conclusion that the decrease in ion density is determined by reduced ionization efficiency of neutrals due to decreased electron temperature, which is apparently controlled by low-frequency oscillations. In the presence of oscillations, an electron can no longer remain on the optimal trajectory for energy accumulation in the macroscopic anode-cathode electric field due to scattering. The ion energy spectra *4–6* (Fig. 9) show broadening of distributions toward lower energies — ion heating, which also coincides with the appearance of oscillations at frequencies of 160–200 kHz, which can be assumed to determine this transformation of distributions. This assumption is confirmed by estimating the wavelengths λ of azimuthal oscillations with phase velocity $v_{ph} = \omega / k = f \lambda$ ($\lambda = v_{ph} / f$), providing wave-ion resonance, which can be excited in the AAL plasma. For example, for neon ions with energy $W = 500$ eV and velocity $v \approx 7 \cdot 10^4$ m/s with the length of the average ($R = 9$ cm) circumference of the AAL discharge chamber $L \approx 0.56$ m, if $\lambda_{max} = L$, then the minimum excitable resonant frequency $f_{min} \approx 124$ kHz. Consequently, in the AAL, oscillations with $f \leq 1$ MHz can be attributed to azimuthal oscillations.

In the plasma emission spectra, no new lines of excited atoms appear when the magnetic field changes. Only the intensity of the lines changes, similar to the change in ion density. There are no emission lines of excited singly charged neon ions, which gives an estimate of the upper limit of the electron temperature ~ 30 eV (ion radiation near the wavelength $\lambda = 376.733$ nm). The transition from 470 G $\rightarrow$ 660 G is accompanied by a noticeable decrease in the intensity of all lines (Fig. 10; scan from the Thorlabs OSA interface) in the main emission range of excited neon atoms. The spectra were obtained by recording "in the impinging flow," when the signal from the discharge gap and the near plume of the plasma flow is integrated.

Measurements of emission spectra were also conducted when the spectrometer was oriented across the flow. The plasma at the output of the AAL cathode is still quite dense: the ratio of intensities

along the flow / across the flow, for example, for the 640.1517 nm line $I_L / I_T \approx 3$. The "transverse" spectrum contains all the lines that are in the "longitudinal" spectrum. But the intensity ratios of adjacent lines in these two spectra may differ. For example, for lines 638.5447 nm 1 *1* and 640.1435 nm 2 *2* along the flow $I_1 / I_2 = 2.176$, and across the flow — $I_1 / I_2 = 1.684$. As the magnetic field increases from 720 to 820 G, when recording along the flow, there is a change in the wavelength of plasma emission with maximum amplitude: 640.1399 nm (transition 18.726–20.663 eV) → 585.495 nm (transition 16.848–18.966 eV). At the same time, when recording across the flow, throughout the range of magnetic fields, the wavelength with maximum amplitude remains equal to 640.139 nm. The change in wavelength with maximum amplitude reflects changes occurring inside the discharge gap, namely, a decrease in electron temperature T_e at high magnetic fields, which correlates with the same conclusion obtained from the joint analysis of AFC and ion energy distributions. In the near plume in the decreasing magnetic field, T_e recovers its value.

6. DISCUSSION OF RESULTS

The drift of magnetized electrons relative to unmagnetized ions in plasma **E ×B** discharge leads to excitation of a wide spectrum of oscillations at relative motion velocities $v_d \geq v_{Ti}$, where v_{Ti} is the thermal velocity of ions [16, 17], which is always true for AAL. The maximum angular frequency of oscillations corresponds to $k_y v_d \approx \omega_{pe}$ [18] and for our experimental conditions at $v_d = 2.5 \cdot 10^5$ m/s and $n = 10^{13}$ m^{-3} is of the order of $\omega \leq 1.3 \cdot 10^6$ s^{-1}; $f \leq 2.1 \cdot 10^5$ s^{-1}. In [18], it was also found that narrow regions of electron cyclotron drift instability (ECDI) existence are separated by stability regions, and transitions from stability to instability occur whenever $k_y v_d = n\,\omega_{ce}$ (n is an integer). In our AAL, this determines the wavelengths of ECDI azimuthal oscillations λ = 1–10 cm ($n_1 = 1$; $n_2 = 10$), which is much smaller than the length L. Each resonance corresponds to a specific ratio $k_y v_d / \omega_{pe}$, which can indicate whether oscillations exist or not - whether there will be a peak or trough in the dependence $(\omega_r / \omega_{pe}) = \varphi(k_y v_d / \omega_{pe})$, and when they exist, determine the oscillation frequency. If we take the peak-to-trough step as $\Delta f \sim 0.1\, k_y v_d / \omega_{pe}$ (from Fig. 2 of the cited work; exact comparison is impossible since Fig. 2 is plotted for $\omega_{ce} / \omega_{pe} = 0.1$, while we have $\omega_{ce} / \omega_{pe} \sim 10^2$), then for the range of generated wavelengths $\lambda = 10^{-5}$ m– L the step $\Delta f \sim 1.6 \cdot 10^{11}$ –$2.78 \cdot 10^6$ s^{-1} is too large for our frequency response. Therefore, the jumps in the frequency response of the discharge current in Fig. 6 cannot be explained by the considered effect. For long-wave oscillations with $\lambda \approx L$ (Fig. 8), the distances between clusters of ion current frequency response oscillations of several MHz are characteristic, which fits within the framework of the model described

in [18]. However, its modification is needed to explain the cluster nature of the oscillations. It can be noted that the resonance condition $k_y v_d = n\,\omega_{ce}$ provides a relationship between the oscillation wavelength and macroscopic parameters **E × B** discharge discharge $\lambda \sim Kn^{-1/2}E/B^2$, most strongly, as seen from the experiment, with the magnetic field induction value (K is constant). The increase in B should lead to the appearance of shorter-wavelength high-frequency oscillations, which we observe in the experiment.

In the presence of a finite wave number along the magnetic field, the resonant behavior smooths out, and the wave-particle interaction leads to broadening of the cyclotron resonance. A more acceptable candidate for instability having a component k_r along B_r, is the modified two-stream instability (MTSI) with maximum oscillation amplitude at $k_r \geq k_0$, where k_0 is the azimuthal wave vector [19, 20]. Another property of MTSI, consistent with our results, is the weak, compared to ECDI, decrease in oscillation amplitude in the long-wave range, corresponding to our discharge current oscillation region, with increasing magnetic field.

The fact that in our experiment with $\omega_{ce} \gg \omega_{pi}$ oscillations can be excited at frequencies multiple of the ion plasma frequency ω_{pi} with λ of the order of electron Debye length λ_D, which varies in the range of 0.1-10 cm, also follows from the results of work [21]. For neon, when n changes from 10^6 to 10^7 cm^{-3} the first harmonic of the azimuthal oscillation frequency equals $\omega_{pi} = f_{pi}$ = 300-930 kHz.

As known [17, 22], oscillations excited during ECDI development effectively interact with electrons, particularly increasing their temperature. However, the growth of magnetic field leads to a decrease in the amplitudes of the disturbed electric field of ECDI wave, consequently reducing the contribution of oscillations to electron energy. For our conditions, the electron temperature does not exceed ~ 31 eV - the minimum excitation potential of ions. The emission spectra shown in Fig. 10 do not contain emission lines of excited ions, which indicates the finite capabilities of ECDI in terms of electron heating. Additionally, the increase in magnetic field induction leads to a decrease in oscillation wavelength - an increase in their frequency. Both mentioned effects are qualitatively observed in our experiment.

The results of work [17] also show effective interaction of ECDI oscillations with ions in plasma **E × B** discharge**:** strong spatial azimuthal modulation of density (up to 70%) and energy (up to 100%) of ions can be observed. The cited work discovered oscillations $\omega_E = 2\pi v_d / L$ of notable amplitude, determined by discharge chamber geometry L and drift velocity v_d, with amplitude growing from first to third harmonic. Estimation for our conditions near the cathode (B = 4 kGs; L = 0.565 m) at v

$_d = 2.5 \cdot 10^5$ m/s gives $\omega_{E1} \approx 2.8$ MHz, $\omega_{E2} \approx 2.6$ MHz, $\omega_{E3} \approx 8.4$ MHz - such oscillation frequencies are observed when registering both discharge current and ion current. Near the anode, respectively, $\omega_{Ei} \approx 28$, 56 and 84 MHz, which was not observed in the experiment, therefore it can be concluded that the predominant area of oscillation excitation with frequencies ω_E is the near-cathode region - the zone of high magnetic field values.

The amplitude of the perturbed electric field is large at frequencies of the order of lower hybrid ω_{LH}. For low-density plasma (our case), when $\omega_{ce} / \omega_{pe} \sim 10^{-2}$, the lower hybrid frequency was calculated using the canonical formula $\omega_{LH} = \sqrt{\omega_{Hi}\omega_{He}\left(1+\omega_{Hi}^2/\omega_{pi}^2\right)/\left(1+\omega_{He}^2/\omega_{pe}^2\right)}$ and at $B_{rA} = 340$-990 G, $n = 7.5 \cdot 10^6$-$5.38 \cdot 10^6$ cm^{-3} the linear lower hybrid frequency $f_{LH} = 126$-109 kHz. Such oscillations were mainly registered for the discharge current derivative.

In the inhomogeneous magnetic field of AAL, gradient drift is superimposed on the azimuthal electron drift [23]; azimuthal modulation will also generate modulation in the axial direction.

Measurements of total (DC and AC components) discharge current I_d showed modulation of I_d up to ~ 90% with frequencies f from 6 to 100 kHz. This has been reported in literature for non-self-sustained **E × B** discharges (with external electron source for ignition, discharge maintenance, and ion flow neutralization in the plume) in traditional SPT design and cylindrical ones [24, 25]. Changes in oscillation modes occurred with changes in magnetic or electric fields and working gas flow rate. The cause was attributed to changes in ionization zone configuration, excitation of ionization instability, and nonlinear interaction of different oscillation modes. In explaining the strong discharge current modulation, in our opinion, insufficient attention was paid to the relationship between modulation and efficiency of discharge maintenance by external electron source. Ionization instability in the plasma of our AAL self-sustained discharge is not observed, as the neon ionization degree does not exceed 10^{-4}, i.e., neutral depletion does not occur.

Since ions in AAL move exclusively axially from the point of birth to the cathode, there is a desire to see in the AAL plasma the cause of the excitation of axial electric field oscillations that can interact with ions. Let's assume the maximum wavelength of oscillations equal to the length of the discharge gap: $\lambda_{max} = d \approx 1$ cm. For estimation, let's assume the velocity of neon ions equal to $v_{Ne} \approx 7 \cdot 10^4$ m/s, which corresponds to energy of 500 eV (see Fig. 9), which at resonance equals the phase velocity of oscillations $\omega / k = \omega\lambda / 2\pi$. Then the minimum linear frequency of longitudinal oscillations $f_{min} = 7 \cdot 10^6$ Hz - such frequencies are registered by us (see Fig. 7). When there are 3 λ wavelengths in the discharge gap, we can associate this case with the maximum linear frequency f_{max}

= 21 · 10^{6} Hz, which for the mode in Fig. 8 is also the upper boundary frequency. Thus, for AAL conditions with a broad energy spectrum of ions, we can expect effective interaction of ions with longitudinal oscillations in the range from several MHz to ~ 30 MHz. In AAL, there is a possibility of excitation of axial instability of unmagnetized ion flow, arising due to phase shift in the response of electrons and ions to quasi-neutral electric field perturbation [26]. The wavelength spectrum of this instability is broad: $\lambda \le 2\ \pi\rho_e$, where the electron Larmor radius for AAL plasma (25 eV, 1 kG - middle of discharge gap) $\rho_e \approx 1.7\times10^{-3}$ м $\ll d$. Taking into account diffusion effects with classical or anomalous electron collision frequency in [26], it is shown that modes with high frequencies are excited in plasma - up to tens of ω_{LH}, which lies in the range of experimentally obtained frequency responses (Fig. 7). The presence of equilibrium ion velocity spectrum broadens the range of unstable frequencies, especially strongly at $v_i \sim 10\ \rho_e\ \omega_{LH}$, which for our conditions (25 eV, 2 kG) $v_i \approx 6 \cdot 10^{4}$ m/s, which approximately coincides with our above estimation of velocity $v_{Ne} \approx 7 \cdot 10^{4}$ m/s.

The burst-like double structure of signals from the ion sensor (Fig. 4a,b) with an "internal" period $T_1 \approx 5 \cdot 10^{-8}$ (frequency up to 20 MHz) repeats with a period $T_2 \approx 10^{-7}$ s (Fig. 4c,d). Comparison of low-frequency signals from the Rogowski coil (Fig. 4a) and high-frequency signals from the ion sensor (Fig. 4b) suggests different types of oscillations coexisting in AAL plasma, and consequently, different causes for these oscillations. HF oscillations modulate LF ones, and vice versa. In the discussion, we have already considered two possible candidates. The cause of periodic oscillation damping remains unclear. In work [26], it is shown that along with a strong influence on the oscillation generation frequency, the introduction of equilibrium ion velocity $v_i \sim 10\ \rho_e\ \omega_{LH}$ leads to a rapid decrease in oscillation increment with increasing wavelength. Therefore, low-frequency oscillations in the ion frequency response should be less noticeable, which qualitatively corresponds to experimental data. The "peak-trough" mode for HF oscillations cannot apparently be explained within the framework of finding the generation zone in one place (at fixed magnetic and electric fields and plasma density) of the discharge gap; a different approach is needed. In the work of the authors of this article [27], they reported the observation of stationary spatially limited (axial size on the order of fractions of ρ_e) regions with high axial electric field strength - one or two isomagnetic potential jumps, which are also generators of ion density jumps. In ion energy spectra, this manifests as distribution function bursts in narrow energy ranges. Isomagnetic jumps "move" up or down in energy when the magnetic field induction changes. And in work [26], along the discharge channel, a spatial modulation of $\tilde{n}$ plasma density n_0 was discovered, leading to the formation of quasi-periodic waves with $\tilde{n}/n_0 \sim 1$ and a characteristic scale on the order of several ρ_e, which can also be called moving

isomagnetic jumps. In such cases, qualitatively, the conditions for oscillation excitation, sensitive to the values of magnetic and electric fields and plasma density, may be violated, which will lead to the breakdown of existing oscillations.

Almost axial short-wave modes with frequencies $\omega_{ci} \le \omega \le \omega_{ce}$ (ω_{ci} - ion cyclotron frequency) in the SPT discharge region can develop during the gradient-drift instability development [28] with inhomogeneous profiles of magnetic field and plasma density along the discharge channel. Here, the instability development condition is determined by the relationship between the gradients of magnetic field induction and plasma density - the discharge gap may contain zones of stable and unstable discharge burning. The oscillation level strongly depends on the ratio k_x / k_y (x - along the axis; y - azimuthal direction), which differs at different points in the chamber, as k_x changes in it by approximately 1.6 times.

7. CONCLUSION

Simultaneous measurements were performed of the frequency response characteristics of oscillations at frequencies of 20 kHz-30 MHz of the discharge current derivative and ion current in the plasma of independent **E × B** discharge in an accelerator with anode layer when changing the magnetic field at the anode B_{rA} = 205-1010 G, at the cathode - B_{rK} = 800-4200 G under strong magnetic field conditions. Only variable components of currents were recorded. The frequency response measurement results were analyzed together with ion energy distributions measured in the same discharge modes in the range of 50-1200 eV and plasma emission spectra in the wavelength range of 200-1100 nm.

Oscillations have both regular character and irregular bursts. Common features of the frequency response for both currents include multiple frequencies and mostly cluster-like oscillations. When B_{rA} changes from 660 G to 720 G, there is a rapid increase in the frequency of oscillations with maximum amplitude up to $f_{max} \sim$ 4.5 MHz, which remains unchanged until $B_{rA} \approx$ 820 G. Individual powerful peaks at specific frequencies serve as indicators of changes in oscillation excitation mode when the magnetic field changes. In the low-frequency region (not exceeding 1 MHz), a threshold magnetic field of $B_{rA} \approx$ 720 G can be identified, at which sharp jumps in frequency response toward higher frequencies occur: discharge current oscillations at 43 kHz disappear but appear at 331 kHz; distinct peaks of ion current oscillations at 43 and 87 kHz also disappear but oscillation bursts appear at frequencies of 331 and 622 kHz. At $B_{rA} \ge$ 720 G, the frequency responses of both currents have oscillation clusters with some distinct peaks.

The frequency response of the discharge current has approximately 5 times lower oscillation frequencies $f_{\max}$ with maximum amplitude than the ion current oscillation frequencies at $205 \le B_{rA} \le 660$ G. When B_{rA} becomes greater than 820 G, there is a sharp decrease in $f_{\max}$ for the discharge current frequency response, but a sharp increase in $f_{\max}$ for the ion current frequency response.

The observed decrease in intensity of all emission lines of excited neon atoms with increasing B_{rA} from 470 to 660 G can be attributed to the emergence of electrostatic oscillations in discharge and ion currents. Additionally, a sharp decrease in ion density is registered, occurring due to reduced ionization efficiency of neutrals, which at constant working pressure of neon is determined by the decline in electron energy. The main energy gain by electrons occurs during their movement along the stationary electric field between anode and cathode. Electric field oscillations reduce the portion of the path traveled by electrons along the field, deflecting particles at the mean free path from the optimal trajectory, limiting the final energy. An increase in electron temperature to values of $T_e > 30$-35 eV during interaction with oscillations does not occur.

The broad spectrum of oscillations in AAL plasma indicates the fulfillment of conditions for exciting various instabilities. Thus, one possible explanation for discharge current oscillations with frequencies $f \le 200$ kHz could be MTSI [19, 20], where there is no strict requirement for purely radial magnetic field. Besides frequency correspondence, another MTSI property consistent with our results is the weak sensitivity of oscillation amplitude to magnetic field increase. Parameters of ECDI azimuthal oscillations [17, 18] explain the frequencies of ion current oscillations $f \le 1$ MHz and the appearance of short-wave high-frequency oscillations with increasing magnetic field.

Longitudinal oscillations with frequencies from several MHz to ~ 30 MHz, which are excited during the development of axial instability of unmagnified ion flow [26] and gradient-drift instability [28], can effectively influence ions. The "peak-trough" mode for oscillations with $f \ge 1$ MHz can be understood if we assume that during measurements, the oscillation generation zone either changed its position, moving to an area with different fields and density, or the fields and plasma density changed at a fixed location. Such an explanation is not contradictory if we consider isomagnetic jumps [27] or quasi-periodic waves with $\tilde{n}/n_0 \sim 1$ and a characteristic scale of several ρ_e [26] as areas with special parameter changes, where oscillation excitation conditions, sensitive to magnetic and electric field values and plasma density, can change, leading to either disruption or excitation of oscillations.

REFERENCES

1. *Lashmore-Davies C.N.*, *Martin T.J.* // Nucl. Fusion. 1973. V. 13. P. 193. Doi: 10.1088/0029-5515/13/2/007.
2. *Choueiri E.Y.* // Phys. Plasmas. 2001. V. 8. P. 1411. Doi: 10.1063/1.1354644.
3. *Smolyakov A.I.*, *Chapurin O.*, *Frias W.*, *Koshkarov O.*, *Romadanov I.*, *Tang T.*, *Umansky M.*, *Raitses Y.*, *Kaganovich I.D.*, *Lakhin V.P.* // Plasma Phys. Control. Fusion. 2017. V. 59. P. 014041. Doi: 10.1088/0741-3335/59/1/014041.
4. *Boeuf J.-P.*, *Smolyakov A.* // Phys. Plasmas. 2023. V. 30. P. 050901. Doi: 10.1063/5.0145536.
5. *Morozov A.I.*, *Esipchuk Y.V.*, *Kapulkin A.*, *Nevrovskii V.*, *Smirnov V.A.* // Sov. Phys. Tech. Phys. 1972. V. 17. P. 482.
6. *Esipchuk Yu.V .*, *Morozov A.I .*, *Tilinin G.N .*, *Trofimov A.V .* // Zh. Tekh. Fiz. 1973. V. 43 P. 1466.
7. *Tilinin G.N.* // Sov. Phys. Tech. Phys. 1977. V. 22. P. 974.
8. *Litvak A.A.*, *Raitses Y.*, *Fisch N.J.* // Phys. Plasmas. 2004. V. 11. P. 1701. Doi: 10.1063/1.1634564.
9. *Khmelevskoi I.A.*, *Tomilin D.A.* // Plasma Phys. Rep. 2020. V. 46. P. 563. Doi: 10.1134/S1063780X20050050.
10. *Khmelevskoi I.A., Shashkov A.S., Kravchenko D.A., Tomilin D.A., Krivoruchko D.D.* // Plasma Phys. Rep. 2020. V. 46. P. 627. Doi: 10.1134/S1063780X20060033.
11. *Esipchuk Yu.V.*, *Tilinin G.N.* // ZhTF. 1976. V. 46. P. 718.
12. *Von W. Rogowski, Steinhaus W.* // Arch. Elektrotech. 1912. B. 1. Z. 141. Doi: 10.1007/BF01656479.
13. *Bardakov V.M.*, *Ivanov S.D.*, *Kazantsev A.V.*, and *Strokin N.A.* // Rev. Sci. Instrum. 2015. V. 86. P. 053501. Doi: 10.1063/1.4920998.
14. *Rigin A.V.*, *Strokin N.A.* // Computer Program State Registration Certificate 2022683136. 01.12.2022.
15. *Bardakov V.M.*, *Ivanov S.D.*, *Kazantsev A.V.*, *Strokin N.A.* // Instrum. Exp. Tech. 2015. V. 58. P. 359. DOI: 10.1134/S0020441215030045.
16. *Sizonenko V.L.* and *Stepanov K.N.* // Nucl. Fusion. 1967. P. 131. Doi: 10.1088/0029-5515/7/2-3/007.
17. *Janhunen S.*, *Smolyakov A.*, *Chapurin O.*, *Sydorenko D.*, *Kaganovich I.*, *Raitses Y.* // Phys. Plasmas. 2018. V. 25. P. 011608. Doi: 10.1063/1.5001206.

18. *Ducrocq A*., *Adam J.C*., *Heron A*., *Laval G*. // Phys. Plasmas. 2006. V. 13. P. 102111. Doi: 10.1063/1.2359718.
19. *Reza M*., *Faraji F*., *Knoll A*. // Phys. Plasmas. 2024. V. 31. P. 032120. Doi: 10.1063/5.0176581.
20. *Reza M*., *Faraji F*., *Knoll A*. // Phys. Plasmas. 2024. V. 31. P. 032121. Doi: 10.1063/5.0176586.
21. *Cavalier J*., *Lemoine N*., *Bonhomme G*., *Tsikata S*., *Honore C*., *Gresillon D.* // Phys. Plasmas. 2013. V. 20. P. 082107. Doi: 10.1063/1.2359718.
22. *Smolyakov A*., *Zintel T*., *Couedel L*., *Sydorenko D*., *Umnov A*., *Sorokina E*., *Marusov N*. // Plasma Phys. Rep. 2020. V. 46. P. 496. Doi: 10.1134/S1063780X20050086.
23. *Wong H.V*. // Phys. Fluids. 1970. V. 13. P. 757. Doi: 10.1063/1.1692983.
24. *Yamamoto N*., *Nakagawa T*., *Komurasaki K*., *Arakawa Y*. // 27 Int. Electric Propulsion Conf., Pasadena, 2001. IEPC-01-055.
25. *Polzin K.A*., *Sooby E.S*., *Raitses Y*., *Merino E*., *Fisch N.J*. // 31 Int. Electric Propulsion Conf., Ann Arbor, 2009. IEPC-2009-122.
26. *Koshkarov O*., *Smolyakov A.I*., *Romadanov I.V*., *Chapurin O*., *Umansky M.V*., *Raitses Y*., *Kaganovich I.D*. // Phys. Plasmas. 2018. V. 25. P. 011604. Doi: 10.1063/1.5017521.
27. *Strokin N.A*., *Kazantsev A.V*., *Bardakov V.M*., *Thang The Nguyen*, *Kuzmina A.S*. // Phys. Plasmas. 2019. V. 26. P. 073501. Doi: 10.1063/1.5093778.
28. *Marusov N.A*., *Sorokina E.A*., *Lakhin V.P*., *Ilgisonis V.I*., *Smolyakov A.I*. // Plasma Sources Sci. Technol. 2019. V. 28. P. 015002. Doi: 10.1088/1361-6595/aae23d.

FIGURE CAPTIONS

Рис. 1. Fragment of AAL construction: $\delta = 6$ mm; $\Delta \approx 10$ mm; $H \approx 14$ mm — electron emission area from cathode surface (a); $B_r = f(z)$ on the discharge gap axis (b).

Рис. 2. Frequencies with maximum amplitudes; curve *1* (blue) - information from Rogowski coil; *2* (red) - from ion sensor; $q_{Ne} = 100$ cm^3/min, $U_d = 900$ V.

Рис. 3. Amplitude-frequency characteristics of signals from Rogowski coil (curve *1* ; black) and ion collector (curve *2* ; red). The numerical values of discharge and ion current oscillation amplitudes are different due to different nature and sensitivity of the sensors used. $B_{rA} = 910$ G; $q_{Ne} = 100$ cm^3/min, $U_d = 900$ V; distance between adjacent AFC points $\Delta f = 40$ kHz.

Рис. 4. Fragments of oscillograms from Rogowski coil (a, c) and ion current sensor (b, d): $q_{Ne} = 100$ cm^3/min, $U_d = 900$ V; $B_{rA} = 910$ G (a, b); $B_{rA} = 660$ G (c, d).

Рис. 5. Fragments of regular signal oscillograms from ion current sensor (a) and Rogowski coil (b); AFC of signal from ion sensor (c); $q_{Ne} = 100$ cm^3/min, $U_d = 1100$ V, $B_{rA} = 720$ G.

Рис. 6.AFC of signal from Rogowski coil: *1* (black) $B_{1\,rA} = 660$ G; $f_1 \approx 43$ kHz; *2* (red) $B_{2\,rA} = 720$ G; $f_2 \approx 331$ kHz; *3* (blue) $B_{1\,rA} = 820$ G; f_3 - cluster 150-220 kHz with maximum amplitude at 179 kHz. $q_{Ne} = 100$ cm^3/min, $U_d = 1100$ V. Distance between adjacent AFC points is 1 kHz.

Рис. 7. Change in frequency response of ion current oscillations with increasing B_{rA} ; $q_{Ne} = 100$ cm^3/min, $U_d = 1100$ V. At the cathode, respectively, $B_{rK\,1} = 2070$ G, $B_{rK\,2} = 2860$ G, $B_{rK\,3} = 3200$ G, $B_{rK\,4} = 3570$ G, $B_{rK\,5} = 3830$ G. For better visualization, the frequency response amplitudes are multiplied by different coefficients.

Рис. 8. Change in frequency response of ion current oscillations in the kilohertz range with increasing B_{rA} ; $q_{Ne} = 100$ cm^3/min, $U_d = 1100$ V. Discharge currents are 23 mA (*1*), 24 mA (*2*), 30 mA (*3*) and 32 mA (*4*). Amplitude *1* is multiplied by 4.

Рис. 9. Ion energy distributions and ion density (inset): *1* — $B_{rA} = 340$; *2* – 470; *3* — 660; *4* — 820; *5* — 870; *6* — 910 G; $P = 1.2 \cdot 10^{-4}$ Torr, $U_d = 1200$ V, $q_{Ne} = 100$ cm^3/min.

Рис. 10. Neon plasma emission spectra: $P = 1.2 \cdot 10^{-4}$ Torr, $U_d = 1200$ V, $q_{Ne} = 100$ cm^3/min.

Figures

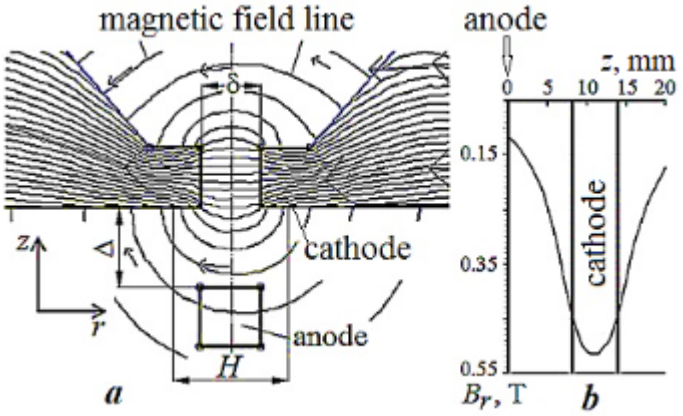

Fig. 1.

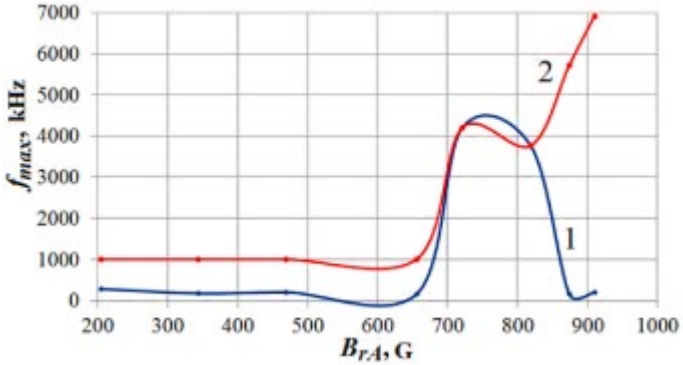

Fig. 2.

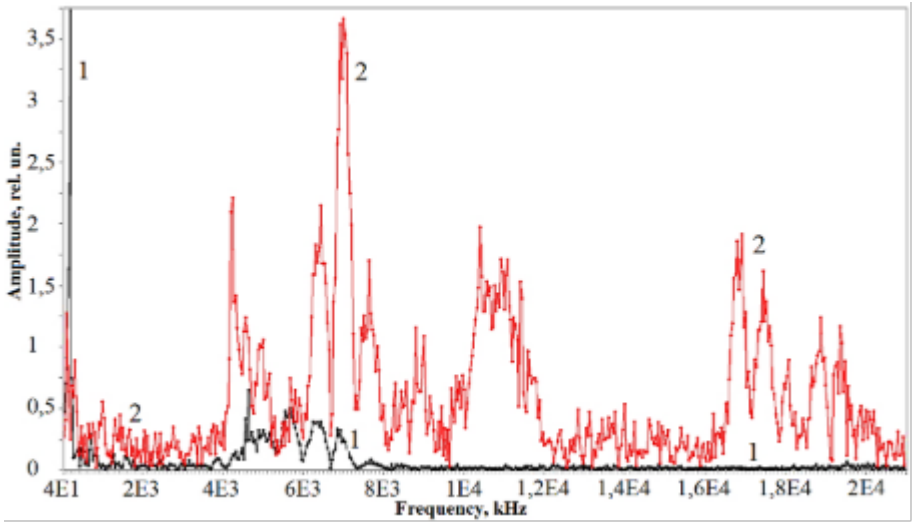

Fig. 3.

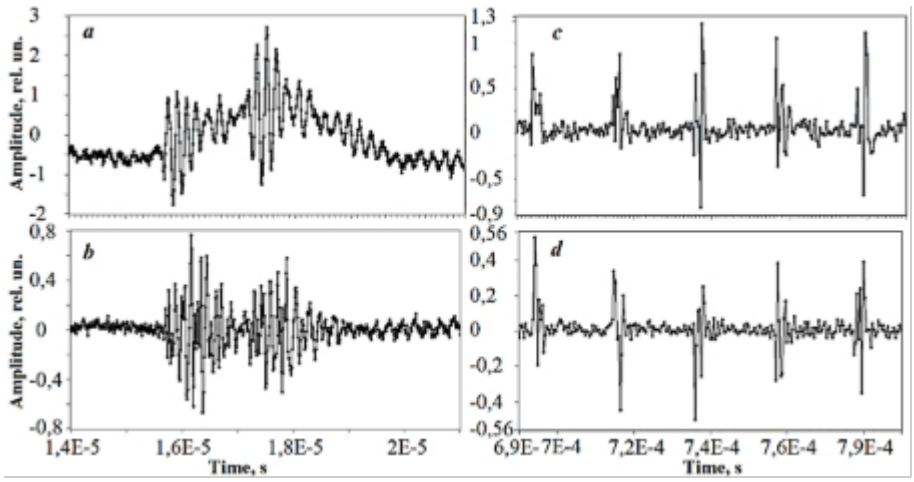
a
b
c
d
Amplitude, rel. un.
Amplitude, rel. un.
Time, s
Time, s
1,4E-5
1,6E-5
1,8E-5
2E-5
6,9E-7E-4
7,2E-4
7,4E-4
7,6E-4
7,9E-4

Fig. 4.

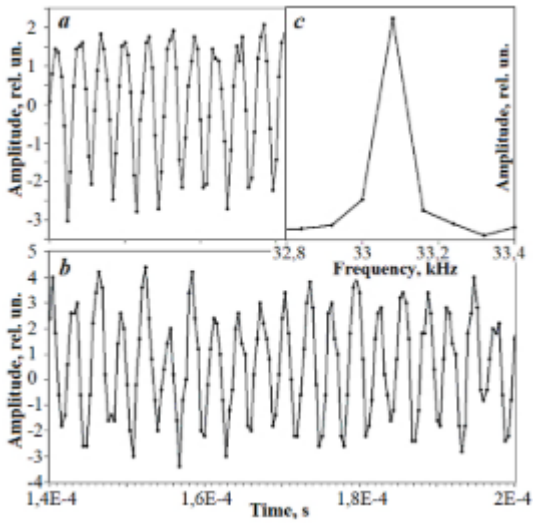
a
b
c
Amplitude, rel. un.
Amplitude, rel. un.
Amplitude, rel. un.
Frequency, kHz
Time, s
32,8
33
33,2
33,4
1,4E-4
1,6E-4
1,8E-4
2E-4

Fig. 5.

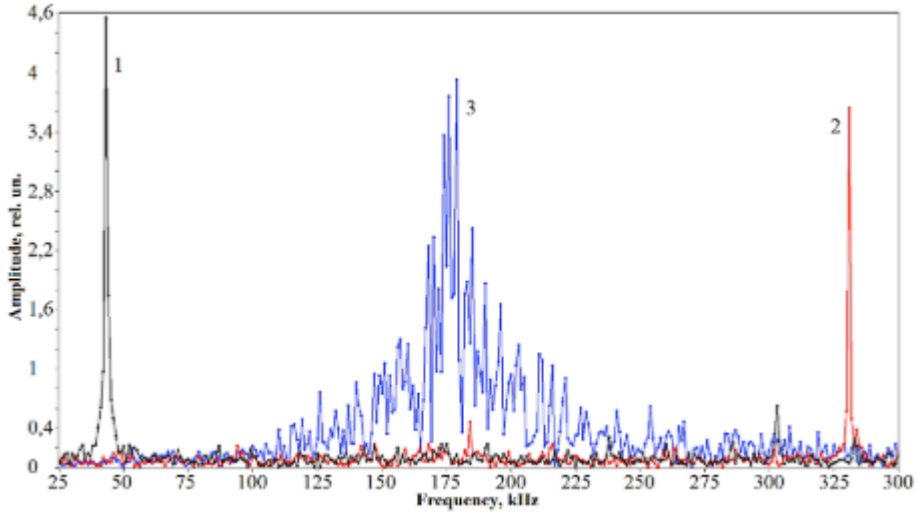
1
2
3
Amplitude, rel. un.
Frequency, kHz
25
50
75
100
125
150
175
200
225
250
275
300
325
300

Fig. 6.

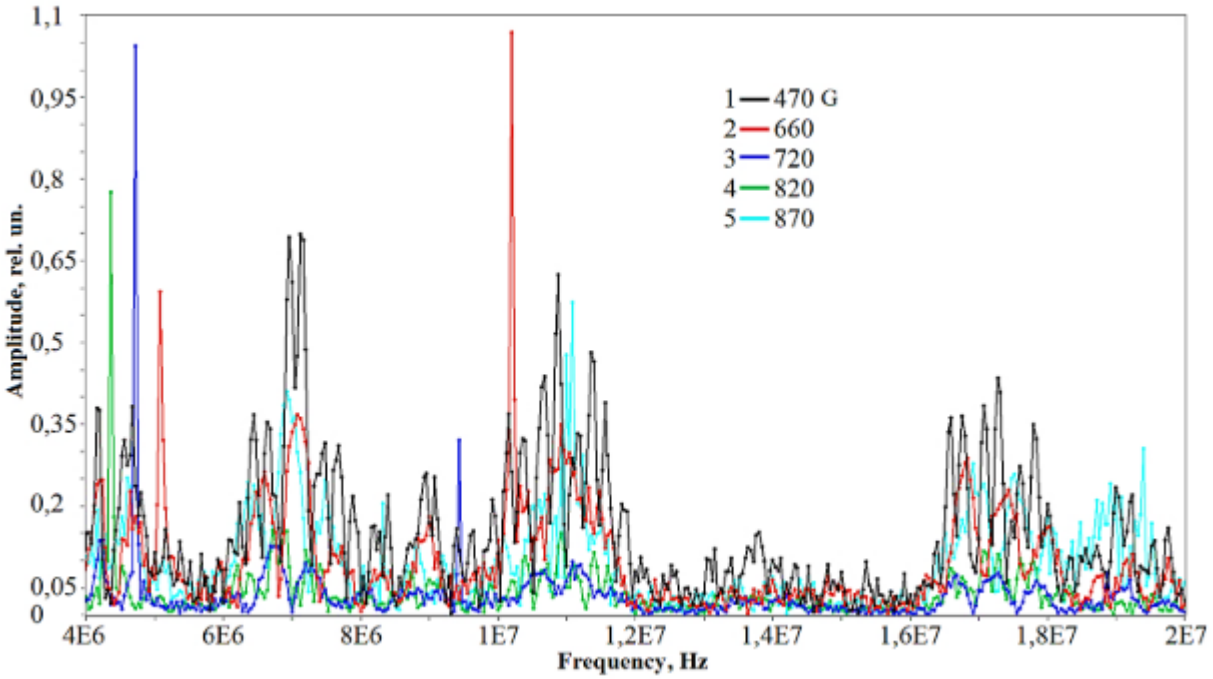

Fig. 7.

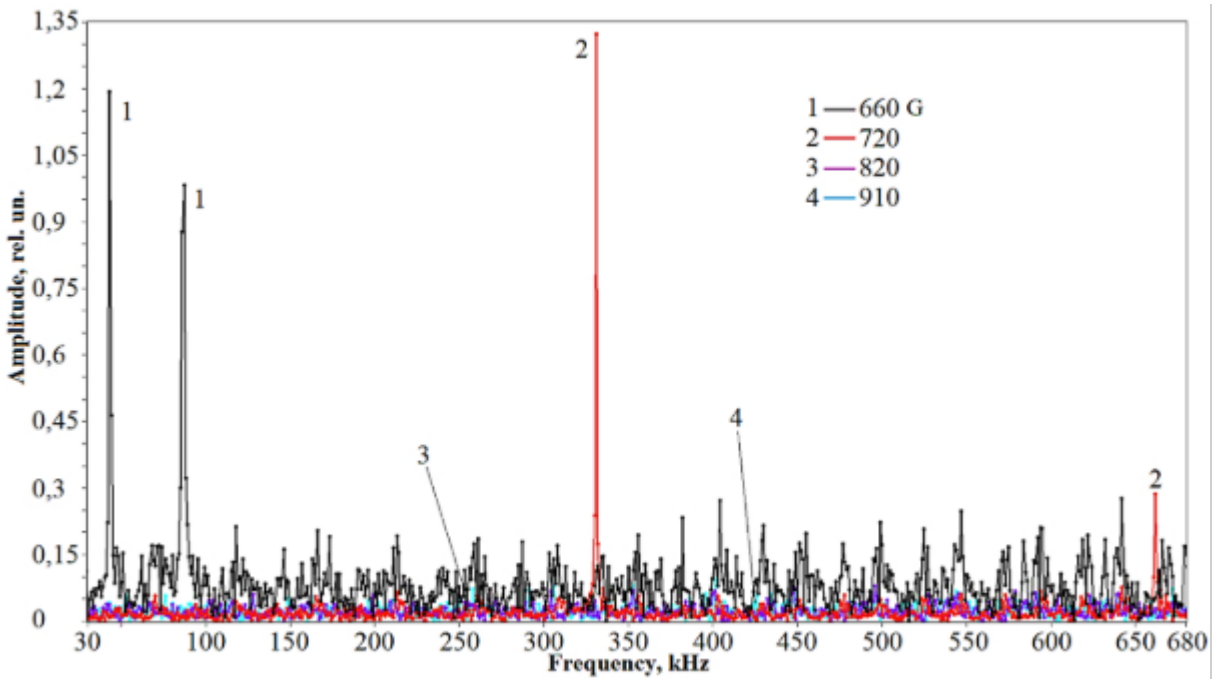

Fig. 8.

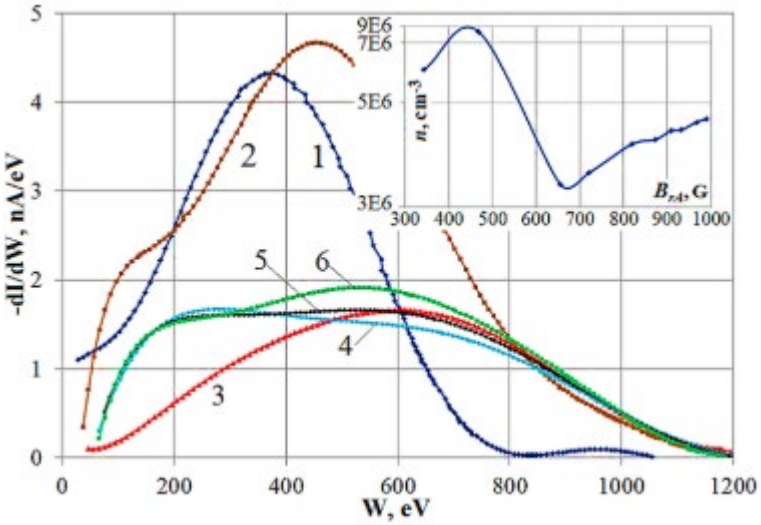
-dI/dW, nA/eV
W, eV
n, cm-3
B_z4, G
1
2
3
4
5
6

Fig. 9.

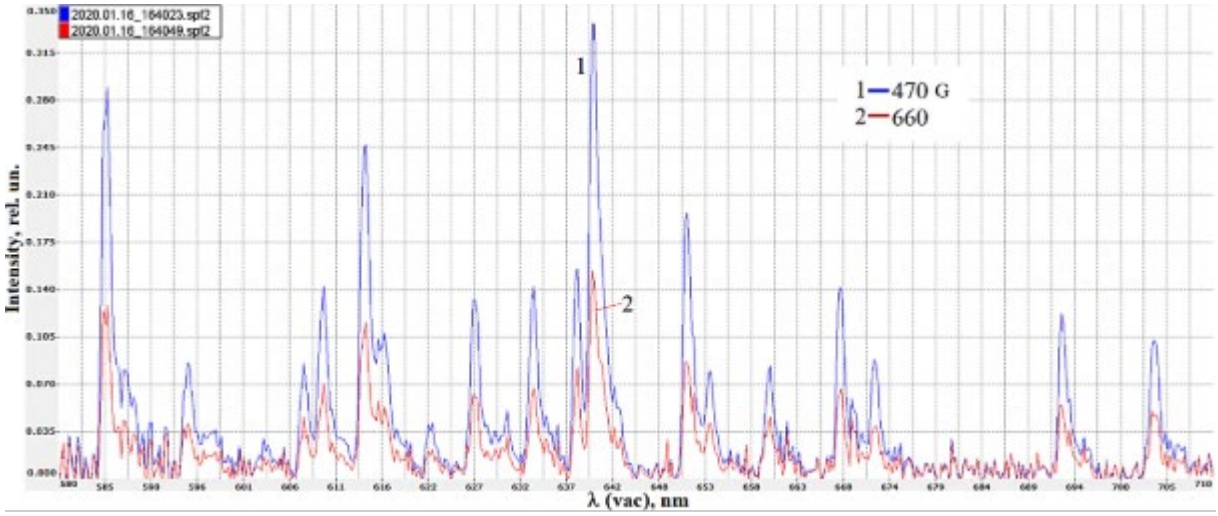
2020.01.16_164023.spt2
2020.01.16_164049.spt2
Intensity, rel. un.
λ (vac), nm
1—470 G
2—660
1
2

Fig. 10.